The Influence of the 1998 El Niño upon Cloud-Radiative Forcing over the Pacific Warm Pool

ROBERT D. CESS AND MINGHUA ZHANG

Marine Sciences Research Center, State University of New York at Stony Brook, Stony Brook, New York

BRUCE A. WIELICKI AND DAVID F. YOUNG

NASA Langley Research Center, Hampton, Virginia

XUE-LONG ZHOU AND YURI NIKITENKO

Marine Sciences Research Center, State University of New York at Stony Brook, Stony Brook, New York

(Manuscript received 25 February 2000, in final form 25 August 2000)

ABSTRACT

Clouds cool the climate system by reflecting shortwave radiation and warm it by increasing the atmospheric greenhouse. Previous studies have shown that in tropical regions of deep convection there is a near cancellation between cloud-induced shortwave cooling and longwave warming. The present study investigates the possible influence of the 1998 El Niño upon this near cancellation for the tropical western Pacific's warm pool; this was accomplished by employing satellite radiometric measurements (Earth Radiation Budget Experiment, and Clouds and the Earth's Radiant Energy System). With the exclusion of the 1998 El Niño, this study also finds near cancellation between the shortwave and longwave cloud forcings and demonstrates that it refers to the average of different cloud types rather than being indicative of a single cloud type. The shortwave cooling slightly dominates the longwave warming, and there is considerable interannual variability in this modest dominance that appears attributable to interannual variability of tropopause temperature. For the strong 1998 El Niño, however, there is a substantially greater tendency toward net radiative cooling, and the physical mechanism for this appears to be a change in cloud vertical structure. For normal years, as well as for the weaker 1987 El Niño, high clouds dominate the radiation budget over the warm pool. In 1998, however, the measurements indicate the radiation budget is partially governed by middle-level clouds, thus explaining the net cooling over the warm pool during the 1998 El Niño as well as emphasizing differences between this event and the weaker 1987 El Niño.

1. Introduction

Clouds radiatively cool the climate system through reflection of shortwave (solar) radiation from the system, while they radiatively warm the system by reducing the outgoing longwave (infrared) radiation that increases the atmospheric greenhouse effect. One of the many insights provided by data from the Earth Radiation Budget Experiment (ERBE) involved understanding the role of clouds on the climate system through analyzing top-of-the-atmosphere (TOA) cloud-radiative forcing measurements provided by ERBE (Ramanathan et al. 1989; Harrison et al. 1990). For example, Kiehl and Ramanathan (1990) demonstrated there is a near cancellation between the longwave (LW) and shortwave (SW) components of cloud-radiative forcing (CRF) in tropical deep-convection regions, such that the net CRF is nearly zero; that is, the SW cooling and LW heating by clouds are of similar magnitude but of opposite sign, so that (SW CRF)/(LW CRF) ≈ -1. Subsequent studies that address this issue are provided by Hartmann et al. (1992), Ockert-Bell and Hartmann (1992), Rossow et al. (1995), Zhang et al. (1995), and Chen et al. (2000). Kiehl (1994) explained this near cancellation in the following manner. In tropical deep-convection regions, high clouds that are optically thick for both LW and SW radiation dominate CRF, while it was suggested that the tops of these thick cirrostratus are near the tropical tropopause. Cloud-top height has little impact on SW CRF, whereas it plays a major role on the magnitude of

Corresponding author address: Dr. Robert Cess, Marine Sciences Research Center, State University of New York at Stony Brook, Stony Brook, NY 11794-5000.
E-mail: cess@atmsci.msrc.sunysb.edu

LW CRF; a high cold cloud will have greater LW CRF than a low warm cloud because it emits less LW radiation to space and thus provides greater greenhouse warming. Kiehl (1994) thus suggested that the near cancellation effect is dominated by the tropical tropopause height.

To investigate the possibility that the strong 1998 El Niño might have influenced the relative magnitudes of SW versus LW CRF, we have combined two datasets that provide measurements of CRF at the TOA. One set consists of ERBE measurements made over a 5-yr period (1985–89) and the other CERES (Clouds and the Earth's Radiant Energy System) measurements that comprise ERBE-like measurements for the first 8 months (January–August) of 1998. Thus the ERBE data encompass the 1987 El Niño, while the CERES data include the stronger 1998 El Niño, which persisted until July 1998 (Wong et al. 2000). We first show that during the 1998 El Niño there was a significant increase in the magnitude of the (SW CRF)/(LW CRF) ratio throughout the warm pool of the tropical western Pacific (TWP), an increase that exceeds that typical of interannual variability in other years. We next select a region contained within the warm pool for which sea surface temperature (SST) and the clear-sky TOA emitted LW and reflected SW radiative fluxes were temporally stable. For the five ERBE years attention is directed to the same eight months (January–August) for which CERES data are available. We demonstrate that changes in cloud type (vertical structure) are the probable cause of the increase in magnitude of the SW to LW CRF ratio for the 1998 El Niño.

2. Analysis

a. Cloud-radiative forcing

The 5-yr (January 1985–December 1989) ERBE S-4G data consist of scanner measurements that have been temporally averaged into monthly means and spatially averaged into 2.5° × 2.5° latitude–longitude grids (Barkstrom and Smith 1986). In addition to TOA reflected SW and TOA emitted LW, the S-4G product also provides SW CRF and LW CRF (Ramanathan et al. 1989; Harrison et al. 1990), for which

$$\text{SW CRF} = R - R_C,$$

where R denotes the TOA all-sky reflected SW and R_C that for clear skies, while

$$\text{LW CRF} = F_C - F,$$

where F and F_C, respectively, denote the all-sky and clear-sky TOA emitted LW. Typically SW CRF is negative (cooling) and LW CRF positive (warming). The 8-month (January–August 1998) CERES ES-4G dataset provides scanner measurements, made from the Tropical Rainfall Measuring Mission (TRMM) Satellite, that have been averaged into monthly mean gridded data in the same way as the ERBE data so as to provide continuity of the two datasets. In the following we adopt 8-month means (January–August), providing five (1985–89) ERBE means and one (1998) CERES mean. The ERBE data are from the Earth Radiation Budget Satellite, which was in a 57° orbit relative to the equator, while for the TRRM Satellite the inclination angle is 35°. Thus both satellites sampled throughout the diurnal cycle. Although the CERES data used in the present study precede those currently available, the differences are minimal.

An overview of ERBE and CERES errors for determination of TOA fluxes can be found in Wielicki et al. (1995) for spatial sampling, time sampling, angle sampling, and calibration. A similar analysis for the conditions appropriate to the current study are given briefly below and are used to estimate the uncertainties in the observations used in the figures and tables.

Calibration absolute accuracy of the ERBE LW and SW radiances are estimated at 1% and 2%, respectively, while CERES LW and SW radiance calibration accuracy is estimated as 0.5% and 1% (Lee et al. 1998; Priestley et al. 1999). Studies have compared the consistency of the ERBE and CERES fluxes using several independent approaches. Currey and Green (1999) compared ERBE and CERES deep convective cloud reflectances for clouds with brightness temperatures less than 205 K and found consistency to within 2%. Wong et al. (2000) compared CERES and ERBE clear-sky LW fluxes in the Tropics and found tropical mean differences of less than 1 W m^{-2} at the end of the 1998 ENSO event in August of 1998. The same study found 1998 ENSO regional and month-to-month differences in January–July 1998 that were consistent with SST and water vapor anomalies taken from NCEP analyses. Finally, the 15-yr record of the active cavity nonscanning wide-field-of-view SW and LW flux data from the ERBS spacecraft allows an overlapping comparison of ERBE and CERES fluxes. Wielicki et al. (1999) compared tropical mean (20°S–20°N) LW fluxes, where monthly mean diurnal sampling error is roughly 0.2 W m^{-2} (1 standard deviation), and found consistency to about 1 W m^{-2} in ERBE (1985–89) and CERES (1998) scanner data overlapped with the ERBS nonscanner data record. The SW overlap record is also consistent, but the tropical mean diurnal sampling error for single months is 2 W m^{-2}. For the present study, we conclude that the all-sky ERBE and CERES broadband radiances are consistently calibrated to within 2% or better for SW fluxes and to within 1% or better for LW fluxes. Since the typical magnitude of both SW and LW cloud-radiative forcing in the current study is $\sim$ 60 W m^{-2}, these calibration uncertainties would lead to uncertainties in SW CRF of 1.2 W m^{-2}, and in LW CRF of 0.6 W m^{-2}.

Time sampling errors have been estimated for monthly and seasonal averages of the regional fluxes following the analysis method of Young et al. (1998) using hourly geostationary data. Seasonal mean fluxes have a diurnal

sampling uncertainty of 1.6 W m^{-2} for regional LW fluxes and 5 W m^{-2} for regional SW fluxes (1 standard deviation) in the Tropics for 20°S–20°N. For the precessing orbits of ERBS and TRMM, the time sampling error decreases roughly as the square root of the number of months, so that uncertainties for the 8-month average results used in this study are estimated at 1 and 3 W m^{-2} for LW and SW fluxes, respectively.

Angle sampling errors will be similar for the ERBS and TRMM precessing orbits as a result of the similar angular sampling for these two orbits in solar zenith, viewing zenith, and viewing azimuth. Therefore this is not expected to be a significant error source when comparing 4- and 8-month averages of ERBS and TRMM fluxes. Spatial sampling errors for regional monthly means are less than 0.5 W m^{-2} for both ERBE and CERES observations.

The NET CRF is simply the sum of the SW and LW components; that is,

$$\text{NET CRF} = \text{SW CRF} + \text{LW CRF}, \qquad (1)$$

so that cancellation between SW CRF cooling and LW CRF warming (NET CRF = 0) can be expressed by the ratio

$$N = -(\text{SW CRF})/(\text{LW CRF}) = 1. \qquad (2)$$

If $N > 1$, then SW cooling dominates. Ramanathan and Collins (1991) evaluated N from the slope of the linear regression of SW CRF versus LW CRF using ERBE data. For a variety of time periods and regions, they found that $0.87 < N < 1.13$ for spatial and seasonal change, while $1.11 < N < 1.33$ when considering flux changes that occurred during the 1987 El Niño relative to normal periods.

Estimates of the uncertainty in observations of NET CRF and N, as defined above, can be made by combining the individual error sources discussed earlier. We assume that time sampling, spatial sampling, and calibration errors are independent. We further assume that SW and LW errors are independent. The final result is an estimated uncertainty (1 standard deviation) for NET CRF defined in Eq. (1) of 4.7 W m^{-2} for 4-month averages and of 3.5 W m^{-2} for 8-month averages. The corresponding uncertainty (1 standard deviation) in the cloud-forcing ratio N, defined in Eq. (2), is 8% for 4-month averages and 6% for 8-month averages. Since the errors in all cases are dominated by time sampling errors for SW fluxes, the assumptions of error independence will have little effect on the final error estimate.

Figure 1a demonstrates that for a normal year $N \approx 1$ throughout most of the tropical Pacific, whereas its magnitude is somewhat increased over some regions during the 1987 El Niño (Fig. 1b). For the stronger 1998 El Niño, however, this increase is more widespread and extends over much of the tropical Pacific as demonstrated in Fig. 1c. To address these differences, we have selected a geographical region within the Pacific warm pool that is centered about the equator from 5°N to 5°S and extends from 140°E–165°E. This region was chosen because interannual variability in SST (the SSTs are available from the Climate Analysis Center, http://ingrid.ldeo.columbia.edu/), spatially averaged over this region and temporally averaged over each of the six 8-month periods, is constant to within ±0.2°C. There is likewise year-to-year consistency, again over the six 8-month periods, in the TOA clear-sky emitted LW to within ±0.8 W m^{-2}, and to within ±0.6 W m^{-2} for the TOA clear-sky reflected SW, which means two things. First, the consistency over the 5-yr ERBE period indicates a lack of interannual variability of the clear-sky TOA radiative fluxes within the 5-yr record of 8-month means for this region, suggesting that we should not expect a significant difference in 1998 relative to the 5-yr ERBE period as is indeed the case. And second, the ERBE–CERES clear-sky LW and SW consistencies are a realistic indication of measurement consistency between the two datasets as previously discussed.

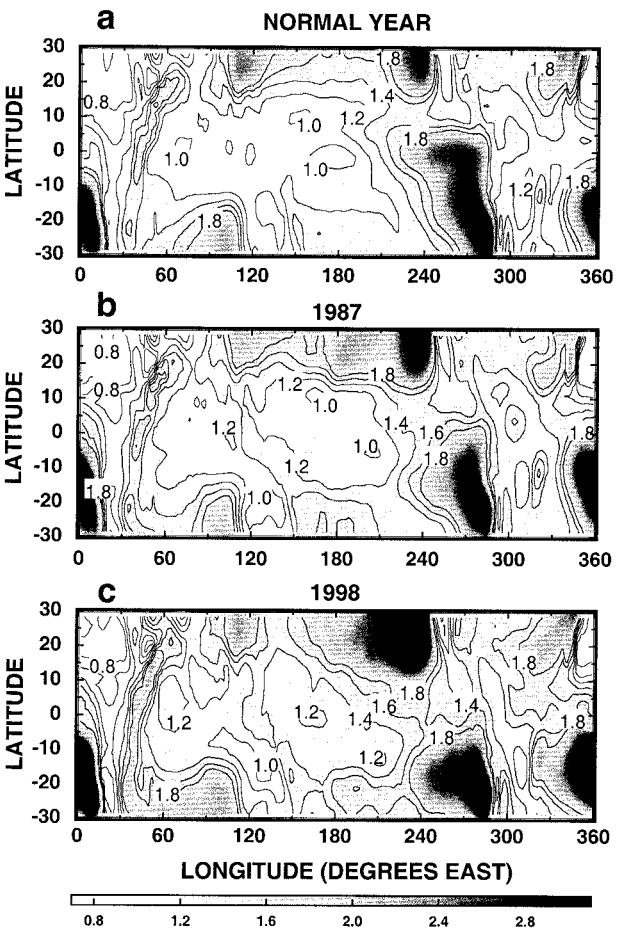

FIG. 1. The geographical distribution of the ratio $N = -(\text{SW CRF})/(\text{LW CRF})$. (a) Normal year, (b) 1987 El Niño, (c) 1998 El Niño.

b. 1998 versus the other years

The SW and LW CRFs, averaged over the selected region of the warm pool, and as a function of mea-

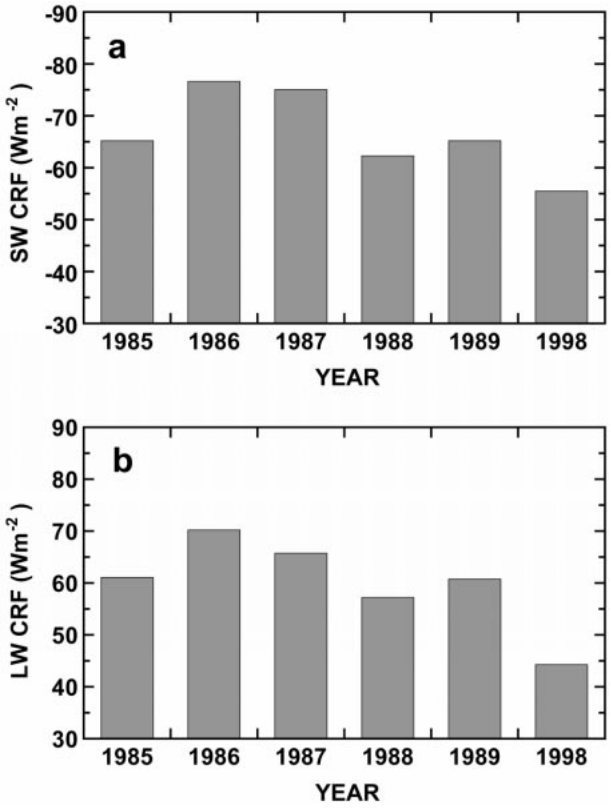

FIG. 2. (a) Eight-month means of the SW CRF for the selected region of the warm pool and for each of the six years. (b) The same as (a) but for the LW CRF.

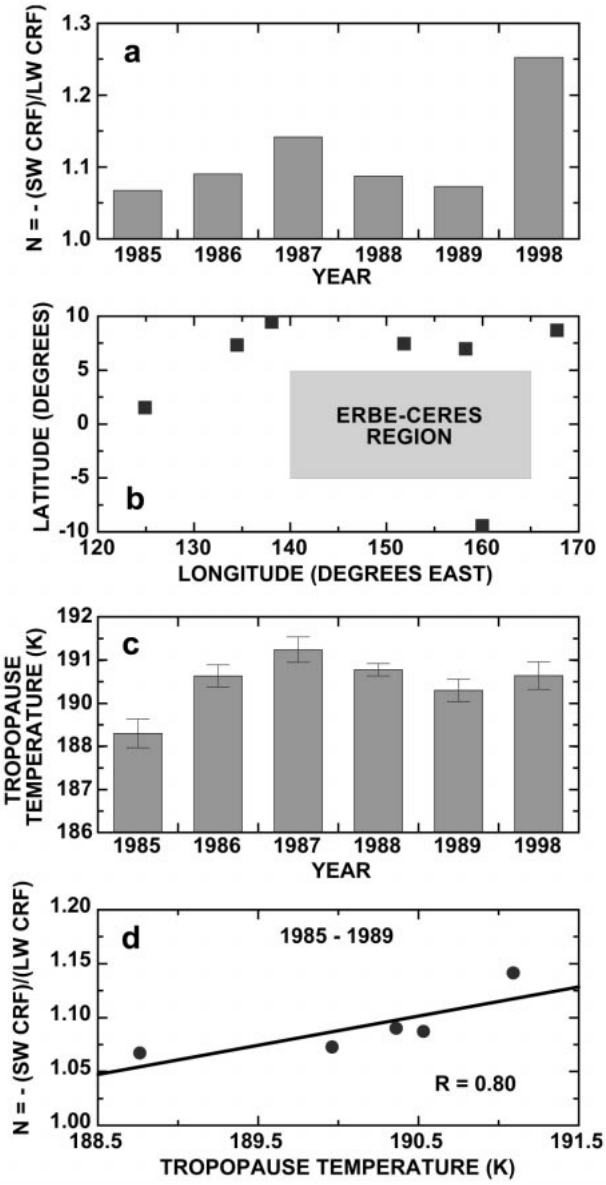

FIG. 3. (a) Eight-month means of the ratio $N = -(\text{SW CRF})/(\text{LW CRF})$ for the selected region of the warm pool and for each of the six years. (b) The locations of the seven sounding stations relative to the selected region of the warm pool. (c) The spatially averaged tropopause temperature for each of the six years. The vertical bars denote one standard deviation of the seven-station tropopause temperatures. (d) Scatterplot of N versus tropopause temperature for the five ERBE years.

surement period, are shown in Figs. 2a and 2b, respectively. Figure 3a, in turn, demonstrates the near cancellation of the SW and LW components of CRF ($N \approx 1.08$) for the normal years (1987 and 1998 excluded). As for the tropical Pacific in general (Fig. 1), N is considerably enhanced during the 1998 El Niño. If this enhancement is associated with that specific event, we should anticipate that the enhancement be greatest during the first few months of 1998, since this El Niño began to dissipate in the spring of 1998 and had essentially ended by late July. This in fact is the case, as is shown in Fig. 4 by comparing the first four months (JFMA) of 1998 to the following four months (MJJA), and with reference to the 1985 and 1989 normal periods. This further serves to emphasize that the $N = 1.25$ result in Fig. 3a is not an artifact of ERBE–CERES differences.

The ratio N shows a modest enhancement for the weaker 1987 El Niño (Fig. 3a). If the temperature (height) of the tropical tropopause, as suggested by Kiehl (1994), controls the value of N, then the 1985–89 interannual variability of N could be related to interannual variability of the tropopause temperature. To test this, we have evaluated the tropopause temperature, defined here as the minimum atmospheric temperature, from the average of temperature soundings taken at seven stations surrounding the 5°S–5°N and 140°–165°E study region and averaged over the same 8-month periods as the ERBE–CERES data. The sounding data are described by Dessler (1998) and Zhou et al. (2000). The locations of the seven stations are shown in Fig. 3b and the spatially averaged tropopause temperatures in Fig. 3c. The spatial variability in tropopause temperature over the seven stations is extremely small, as evidenced by the standard deviations shown in Fig. 3c, implying

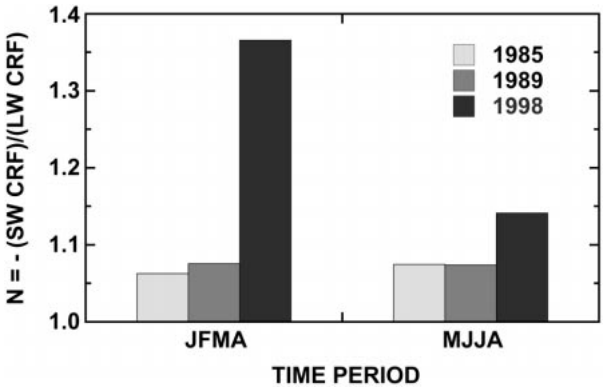

FIG. 4. Four-month means of the ratio $N = -(\text{SW CRF})/(\text{LW CRF})$ for 1985, 1989, and 1998 for the selected region of the warm pool.

that the seven station averages are indicative of the ERBE–CERES region. For the five ERBE years, Fig. 3d suggests that much of the interannual variability of N is related to interannual variability of tropopause temperature. But this cannot explain 1998, for which there is no substantial change in tropopause temperature relative to the other years.

Alternatively, a change in cloud vertical structure (i.e., cloud heights and optical depths) constitutes a possible explanation for 1998 versus the ERBE period. Although cloud radar measurements could address this issue, they are unavailable for the location and time periods in question, and while International Satellite Cloud Climatology Project (ISCCP) data provide information on cloud types, that data are likewise not available for 1998. But much can be learned by understanding the relationship between N and NET CRF, and to this end a broadband radiative transfer model was used to show the dependence of this relationship on cloud altitude and cloud optical depth. The calculations were performed using the 4-stream Fu–Liou radiative-transfer model (Fu and Liou 1993) for a climatological mean tropical atmosphere. The model uses correlated-K fits for gas absorption in 6 solar and 12 thermal infrared wavelength bands covering the broadband reflected solar and emitted thermal radiation. The calculations include Raleigh scattering, aerosol optical depth is set to zero, and the surface albedo is 0.1. The solar zenith angle is set to 60°, and the diurnal average reflected solar radiation is approximated using the diurnal average insolation of 413 W m^{-2} in the Tropics and with cloud albedo evaluated at the 60° solar zenith angle. The intent is to show a reasonable approximation of the results expected, rather than to exactly model any particular case. Results for cloud top altitudes of 15, 9, and 6 km and optical depths ranging from 0.1 to 128 are shown in Fig. 5a, in which SW versus LW CRF cancellation corresponds to the $N = 1$ and NET CRF $= 0$ intercept.

Consider first the cloud top altitude of 15 km. As cloud optical depth increases from a small value (progressing from bottom to top), both cloud emissivity and cloud albedo simultaneously increase, but with the former dominating so that NET CRF increases (net warming). As cloud optical depth continues to increase, this reverses so that cloud albedo increases more rapidly than does cloud emissivity that rapidly asymptotes to unity, ultimately resulting in NET CRF < 0 (net cooling). Within the confines of the model, the 15-km cloud depicted in Fig. 5a can be thought of as representing thin cirrus on the right (small optical depths) to deep-convective (optically thick) clouds at the leftward termination of the curve, and we will shortly elaborate on this termination. Because they are warmer, middle-level clouds, such as those associated with middle-level convection and decaying mesoscale convective systems, have smaller LW CRF, and hence larger N and smaller NET CRF, than do high clouds. The 9- and 6-km clouds depicted in Fig. 5a demonstrate this point, with the latter producing net cooling for all cloud optical depths. Values of N for low clouds, such as marine stratocumulus, can considerably exceed the range given in Fig. 5a. An important point is that the model calculations of Fig. 5a are for a cloud fraction of unity. Kiehl (1994) has shown that N is invariant to cloud fraction, but NET CRF is not. If we had included cloud fraction, then for a point on any of the three curves, there would additionally be a horizontal progression of points with the same value of N, but with NET CRF going to zero as cloud fraction tends to zero.

While Kiehl (1994) suggests $N \approx 1$ for deep-convective (optically thick) clouds, one can reason that this could be revised to $N \approx 1.3$. To demonstrate this revision, recall that N is invariant to cloud amount, and so N can be evaluated from SW and LW CRF that refer to clear skies versus optically thick high clouds. This, of course, will produce CRF magnitudes in excess of those shown in Fig. 2, but it is the ratio in the limit of thick high clouds that is of interest. From the ERBE–CERES measurements for the selected warm pool region, the clear-sky emitted LW at the TOA is about 285 W m^{-2}, while for a cloud-top temperature of 190 K (Fig. 3c) the blackbody emission is 75 W m^{-2}. But there is a small inverse greenhouse effect resulting from emission by CO_2 and ozone in the stratosphere that is warmer than the cloud top, and from a radiative transfer model we estimate this to be 5 W m^{-2}. Thus the emitted TOA LW is 80 Wm^{-2} over deep cold clouds, and the LW CRF, calculated as the difference between clear skies and deep clouds, is thus 205 W m^{-2}. Again from the ERBE–CERES measurements over the selected region, the clear-sky albedo is 0.10, while the TOA insolation for the region (8-month average) is 413 W m^{-2}. In addition, from CERES pixel measurements it has been found that the TOA albedo is 0.74 in the limit of thick cold clouds with infrared brightness temperatures less than 205 K (Hu et al. 1999). The advantage of the new CERES measurements were observations over a complete range of solar zenith angle, viewing zenith angle, and viewing azimuth angle of the anisotropy of solar

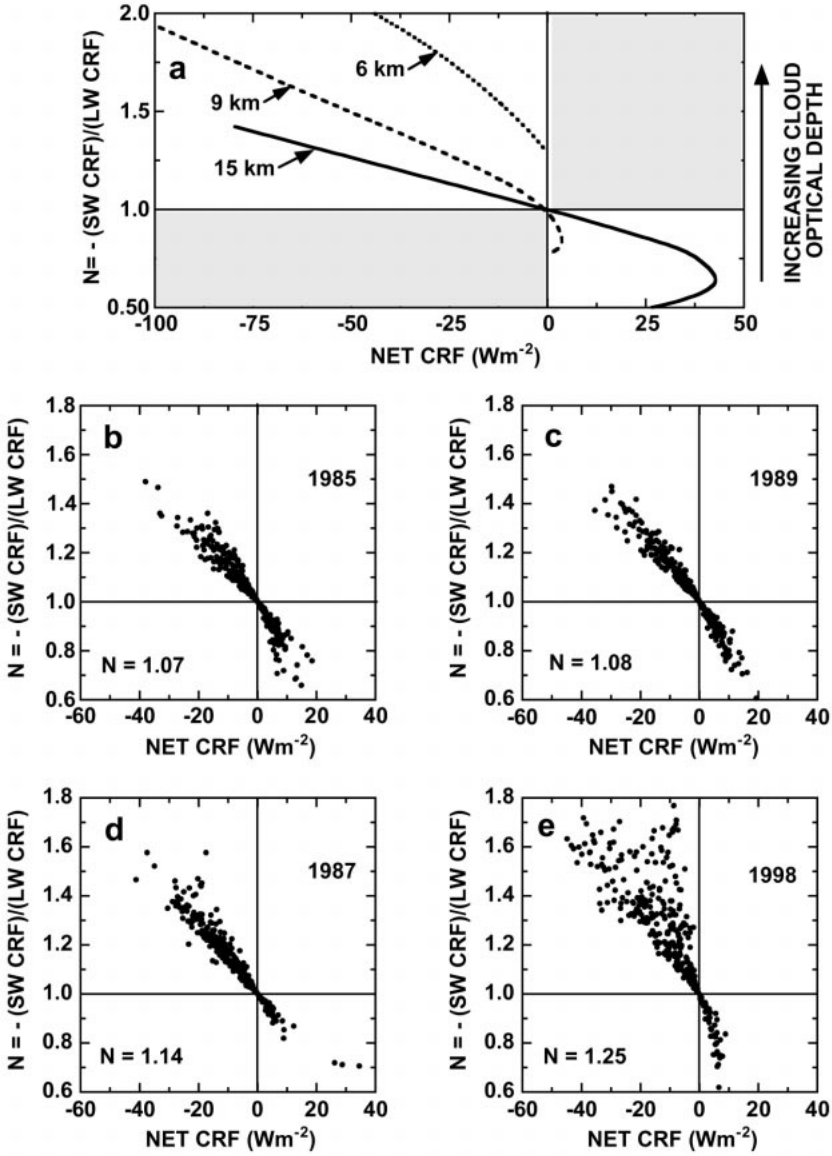

FIG. 5. (a) Model calculations of *N* vs NET CRF for cloud-top altitudes of 15, 9, and 6 km. The shaded areas represent domains that are not physically possible (*N* denoting warming but NET CRF denoting cooling and vice versa). (b) Scatterplot of *N* vs NET CRF for 1985. (c) The same as (b) but for 1989. (d) The same as (b) but for 1987. (e) The same as (b) but for 1998.

radiation for these deep convective clouds. These new observations were used by Hu et al. (1999) to develop more accurate radiance-to-flux conversions specifically for deep convective clouds. An analysis of ERBE reflectances for deep convective clouds colder than 205 K were found to agree with CERES measurements to within 2% when consistent solar illumination and viewing conditions were used (Curry and Green 1999). So SW CRF is -264 W m^{-2} and thus $N = 264/205 \approx 1.3$. This limit is depicted by the leftward termination of the curve in Fig. 5a for the 15-km cloud top, although the model gives a slightly larger value.

Scatterplots of *N* versus NET CRF are given in Figs. 5b and 5c for two normal years and in Figs. 5d and 5e for the two El Niño years. Each point represents an ERBE–CERES monthly mean and 2.5° × 2.5° grid average. Since 40 grids are within the 5°N–5°S and 140°–165°E region, there are 320 data points for each 8-month period. The two normal years (Figs. 5b and 5c) are largely consistent with our expectations from Fig. 5a for high clouds, taking into account that fractional cloud cover will move the data points toward NET CRF = 0. The data points span the range from thin cirrus on the right to deep-convective clouds on the left. Some data

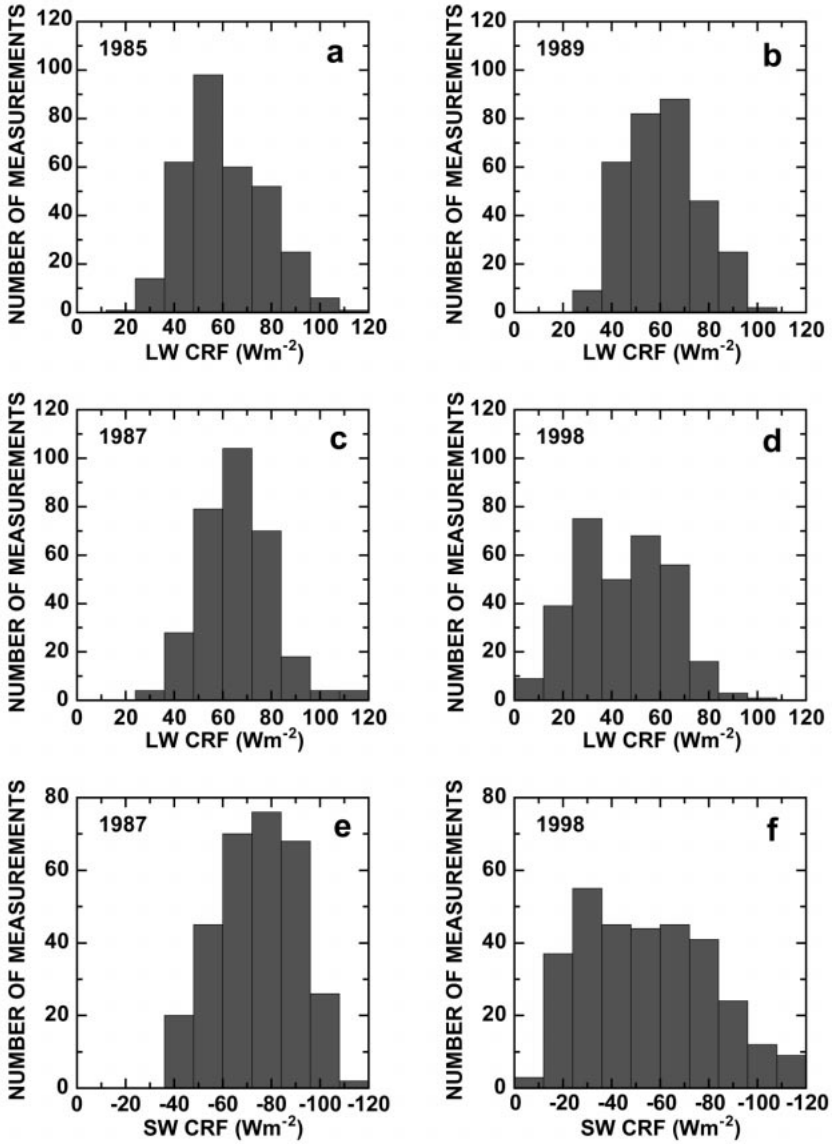

FIG. 6. (a) Frequency distribution of LW CRF for 1985. (b) Same as (a) but for 1989. (c) Same as (a) but for 1987. (d) Same as (a) but for 1998. (e) Frequency distribution of SW CRF for 1987. (f) Same as (a) but for 1998.

to the upper left exceed $N \approx 1.3$ and may be due to middle-level clouds, but if so their populations are small. Moreover, the radiometric measurements cannot preclude the existence of middle-level clouds in conjunction with high-level clouds. It is important to note that the near cancellations, $N = 1.07$ and 1.08, refer to the average of the differing clouds, ranging from thin cirrus to optically thick convective clouds, rather than being indicative of a single cloud type. The data for the 1987 El Niño, shown in Fig. 5d, are not appreciably different than for the two normal years (Figs. 5b and 5c), except there appear to be fewer thin cirrus which, by itself, would increase the average value of *N*. As shown in Fig. 5e, however, the strong El Niño of 1998 is quite different than for the other years. It is again emphasized that any point in Figs. 5b–e is a monthly mean for a $2.5° \times 2.5°$ grid and thus represents an ensemble distribution that is weighted toward higher or lower cloud altitudes. As discussed above, decreases in cloud fraction will tend to move points toward NET CRF = 0 in the figures, while decreases in cloud height will move them up in the figures. This argues that the changes in Fig. 5e, relative to Figs. 5b–d, are in part due to a reduction in average cloud height, since the maximum value of *N* has increased to 1.8 for 1998.

Although we have argued that the scatterplots in Figs. 5b–d span the range from thin cirrus on the right to deep-convective clouds ($N \approx 1.3$) on the left, there does

exist the possibility that middle-level clouds could produce values of N less than 1.3 together with NET CRF < 0 as could be suggested by Fig. 5a. But if this were the case we would anticipate greater horizontal scatter, for NET CRF < 0, than is evidenced in Figs. 5b–d. In any event, comparing these figures to Fig. 5e clearly demonstrates that the contribution of middle-level clouds is certainly more important during the 1998 El Niño.

The frequency distribution of LW CRF further demonstrates significant differences in 1998 as opposed to the other years. As shown in Figs. 6a–d, LW CRF tends to exhibit a bimodal distribution for 1998, with the smaller mode suggestive of middle-level clouds in addition to near-clear conditions that are absent for the other years. Comparison of the SW CRF for 1987 (Fig. 6e) and 1998 (Fig. 6f) again emphasizes the existence of near-clear conditions for the latter period.

c. Summary

Consideration of the results in Figs. 5 and 6 together indicate that the most likely scenario is that in fact both the cloud heights and cloud fractional coverage have decreased in 1998. A decrease in cloud heights is indicated by

1) the drop in frequency of the largest LW CRF events (Fig. 6d vs Figs. 6a and 6b),
2) the increase in the value of N above 1.5 (Fig. 5e vs Figs. 5b and 5c).

The theoretical model calculations shown in Fig 5a indicate that for a given NET CRF value, the effect of lowering cloud height is to increase N. Changes in cloud amount do not affect the value of N, and changes in cloud optical depth primarily move diagonally in Fig. 5a. For the 1998 El Niño period, values of N reach almost 1.8 at a NET CRF of -40 W m^{-2}, while for the same NET CRF value in 1985 or 1989, the maximum value of N is about 1.5. Increases in cloud optical depth are unlikely to explain the increased value of N because the frequency distribution of SW CRF in Fig. 6f shows a distribution shifted to lower values of SW CRF and therefore lower values of cloud optical depth and/or cloud amount. But if only cloud height caused the changes in Fig. 5e, then we would not expect the decreased SW CRF values in the histogram of Fig. 6f. Cloud amount decrease would be consistent with the increased frequency of low values of SW CRF (Fig. 6f) and LW CRF (Fig. 6d), as well as the reductions in magnitude of NET CRF (Fig. 5e), when compared to the equivalent 1985, 1987, or 1989 results. We conclude that the results for the 1998 El Niño indicate both a reduction in cloud altitude as well as a reduction in cloud fraction.

This change in cloud structure is likely a result of the change in SST gradient in the tropical Pacific. SST distributions in the first eight months for a normal year, for 1987, and for 1998 are shown as contours in Figs. 7a–c, respectively. In the normal year, the TWP warm pool extends to the southern Pacific convergence zone in the Southern Hemisphere and to the intertropical convergence zone in the Northern Hemisphere, with a closed 29°C contour in the TWP. In 1987 the warm pool is slightly displaced eastward, but the 29°C contour line is structurally similar to that for a normal year. In 1998, however, the 29°C contour in not closed in the TWP, and the SST is longitudinally more uniform. The SST difference in the zonal direction across the entire tropical Pacific and the Indian Ocean is about 2°C, in contrast to the 4°C difference for a normal year. The associated distributions of the magnitude of the SW CRF are also shown in Fig. 7. It is seen that there is an overall reduction of SW CRF in the tropical Pacific during the 1998 El Niño, consistent with our prior conclusion concerning the specified study region, and presumably related with reduced overall intensity of tropical convection.

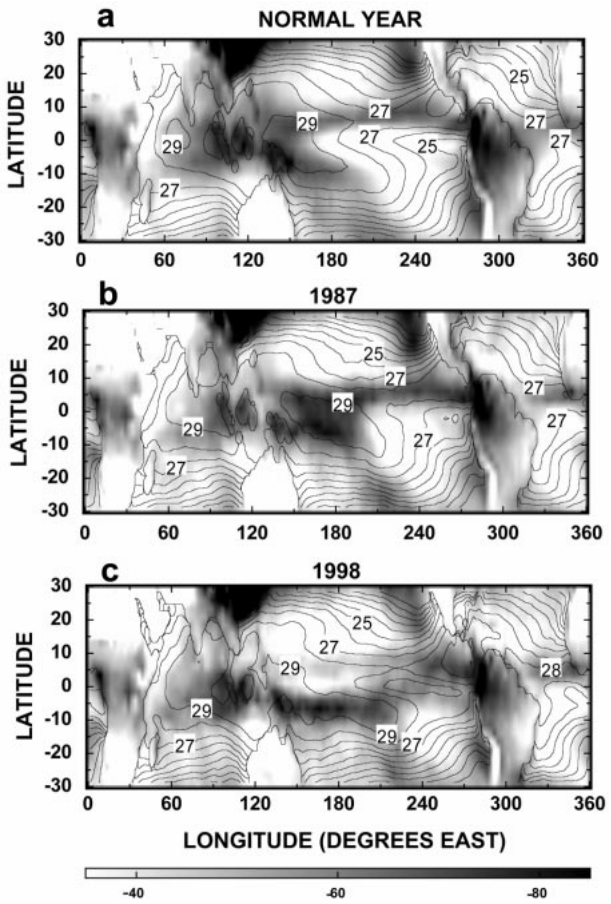

FIG. 7. SST distributions averaged from Jan to Aug (°C, contours) and the corresponding distribution of SW CRF (W m^{-2}, shaded gray images). (a) Normal year, (b) 1987 El Niño, and (c) 1998 El Niño.

3. Conclusions

The primary conclusions of this study are summarized as follows.

- The near cancellation between SW and LW CRF for tropical regions of deep convection ($N \approx 1$), as observed in this and earlier studies, refers to the average of differing cloud types. These range from thin cirrus ($N < 1$) to optically thick convective clouds ($N \approx 1.3$), rather than being indicative of a single high-cloud type.
- For the strong 1998 El Niño, there is a tendency toward net radiative cooling ($N = 1.25$), and the physical mechanism appears to be a change in cloud vertical structure. For normal years as well as 1987, high clouds, ranging from thin cirrus to deep-convective clouds, dominate the radiation budget over the warm pool. During 1998, however, the measurements indicate the radiation budget is partially governed by middle-level clouds, which explains the net cooling over the warm pool during this El Niño. Concurrent with this is a reduction in fractional cloud cover. It is emphasized, however, that these conclusions apply to 1998 and should not be generalized to other El Niños; they certainly are not applicable to 1987.

Acknowledgments. We thank Tom Charlock and Fred Rose for providing easy Web access to the Fu-Liou radiative transfer model for the calculations in Fig. 4a. This work was supported in part by the CERES Project through NASA Contract NAS1-981421 and by the DOE through Grant DEFG0290ER61063 and DEFG028ER6013, both to SUNY Stony Brook.

REFERENCES

Barkstrom, B. R., and G. L. Smith, 1986: The Earth Radiation Budget Experiment—Science and implementation. *Rev. Geophys.,* **24,** 379–390.

Chen, T., W. B. Rossow, and Y. C. Zhang, 2000: Radiative effects of cloud-type variations. *J. Climate,* **13,** 264–286.

Currey, C., and R. N. Green, 1999: Validation of the CERES shortwave measurements over desert and cloud scenes. Preprints, *10th Conf. on Atmospheric Radiation,* Madison, WI, Amer. Meteor. Soc., 567–570.

Dessler, A. E., 1998: A reexamination of the ''stratospheric fountain'' hypothesis. *Geophys. Res. Lett.,* **25,** 4165–4168.

Fu, Q., and K. N. Liou, 1993: Parameterizations of the radiative properties of cirrus clouds. *J. Atmos. Sci.,* **50,** 2008–2025.

Harrison, E. F., P. Minnis, B. R. Barkstrom, V. Ramanathan, R. D. Cess, and G. G. Gibson, 1990: Seasonal variation of cloud radiative forcing derived from the Earth radiation Budget experiment. *J. Geophys. Res.,* **95,** 18 687–18 703.

Hartmann, D. L., M. E. Ockert-Bell, and M. L. Michelsen, 1992: The effect of cloud type on Earth's energy balance: Global Analysis. *J. Climate,* **5,** 1281–1304.

Hu, Y., B. Wielicki, Q. Fu, B. Lin, G. Gibson, and N. Loeb, 1999: Deep convective cloud albedo from TRMM/CERES. Preprints, *10th Conf. on Atmospheric Radiation,* Madison, WI, Amer. Meteor. Soc., 103–105.

Kiehl, J. T., 1994: On the observed near cancellation between longwave and shortwave cloud forcing in tropical regions. *J. Climate,* **7,** 559–565.

——, and V. Ramanathan, 1990: Comparison of cloud forcing derived from Earth Radiation Budget Experiment with that simulated by the NCAR Community climate Model. *J. Geophys. Res.,* **95,** 11 679–11 698.

Lee, R. B., III, and Coauthors, 1998: Prelaunch calibrations of the CERES TRMM and EOS-AM1 spacecraft thermistor bolometer sensors. *IEEE Trans. Geosci. Remote Sens.,* **36,** 1173–1185.

Ockert-Bell, M. E., and D. L. Hartmann, 1992: The effect of cloud type on Earth's energy balance: Results for selected regions. *J. Climate,* **5,** 1157–1171.

Priestley, K. J., R. B. Lee III, R. N. Green, S. Thomas, and R. S. Wilson, 1999: Radiometric performance of the CERES protoflight model on the TRMM spacecraft for 1998. Preprints, *10th Conf. on Atmospheric Radiation,* Madison, WI, Amer. Meteor. Soc., 33–36.

Ramanathan, V., and W. Collins, 1991: Thermodynamic regulation of ocean warming by cirrus clouds deduced from observations of the 1987 El Niño. *Nature,* **351,** 27–32.

——, R. D. Cess, E. F. Harrison, P. Minnis, B. R. Barkstrom, E. Ahmad, and D. Hartmann, 1989: Cloud-radiative forcing and climate: Results from the Earth Radiation Budget Experiment. *Science,* **243,** 57–63.

Rossow, W. B., and Y. C. Zhang, 1995: Calculation of surface and top of atmosphere radiative fluxes from physical quantities based on ISCCP data sets. 2. Validation and first results. *J. Geophys. Res.,* **100,** 1167–97.

Wielicki, B. A., R. D. Cess, M. D. King, D. A. Randall, and E. F. Harrison, 1995: Mission to Planet Earth: Role of clouds and radiation in climate. *Bull. Amer. Meteor. Soc.,* **76,** 2125–2153.

——, T. Wong, D. F. Young, B. R. Barkstrom, R. B. Lee III, 1999: Differences between ERBE and CERES tropical mean fluxes: ENSO, climate change, or calibration? Preprints, *10th Conf. on Atmospheric Radiation,* Madison, WI, Amer. Meteor. Soc., 48–51.

Wong, T., D. F. Young, M. Haeffelin, and S. Weckmann, 2000: Validation of the CERES/TRMM ERBE-like monthly mean clear-sky longwave dataset and the effects of the 1998 ENSO event. *J. Climate,* **13,** 4256–4267.

Young, D. F., P. Minnis, D. R. Doelling, G. G. Gibson, and T. Wong, 1998: Temporal interpolation methods for the Clouds and the Earth's Radiant Energy System (CERES) Experiment. *J. Appl. Meteor.,* **37,** 571–590.

Zhang, Y. C., W. B. Rossow, and A. A. Lacis, 1995: Calculation of surface and top of atmosphere radiative fluxes from physical quantities based on ISCCP data sets. 1. Method and sensitivity to input data uncertainties. *J. Geophys. Res.,* **100,** 1149–1165.

Zhou, X. L., M. A. Geller, and M. H. Zhang, 2001: The cooling trend of the tropical cold point tropopause temperature and it implications. *J. Geophys. Res.,* **106,** 1511–1522.